Transient transition behaviors of fractional-order simplest chaotic circuit with bi-stable locally-active memristor and its ARM-based implementation

Zong-Li Yang(杨宗立), Dong Liang(梁栋), Da-Wei Ding(丁大为), Yong-Bin Hu(胡永兵), and Hao Li(李浩)
Citation: Chin. Phys. B, 2021, 30 (**12**): 120515. DOI: 10.1088/1674-1056/ac1fdf
Journal homepage: http://cpb.iphy.ac.cn; http://iopscience.iop.org/cpb

What follows is a list of articles you may be interested in

Dynamical analysis, circuit realization, and application in pseudorandom number generators of a fractional-order laser chaotic system

Chenguang Ma(马晨光), Santo Banerjee, Li Xiong(熊丽), Tianming Liu(刘天明), Xintong Han(韩昕彤), and Jun Mou(牟俊)
Chin. Phys. B, 2021, 30 (**12**): 120504. DOI: 10.1088/1674-1056/abfbd4

Adaptive synchronization of a class of fractional-order complex-valued chaotic neural network with time-delay

Mei Li(李梅), Ruo-Xun Zhang(张若洵), and Shi-Ping Yang(杨世平)
Chin. Phys. B, 2021, 30 (**12**): 120503. DOI: 10.1088/1674-1056/abfa09

Hidden attractors in a new fractional-order discrete system: Chaos, complexity, entropy, and control

Adel Ouannas, Amina Aicha Khennaoui, Shaher Momani, Viet-Thanh Pham, Reyad El-Khazali
Chin. Phys. B, 2020, 29 (**5**): 050504. DOI: 10.1088/1674-1056/ab820d

A novel color image encryption scheme using fractional-order hyperchaotic system and DNA sequence operations

Li-Min Zhang(张立民), Ke-Hui Sun(孙克辉), Wen-Hao Liu(刘文浩), Shao-Bo He(贺少波)
Chin. Phys. B, 2017, 26 (**10**): 100504. DOI: 10.1088/1674-1056/26/10/100504

Abundant solutions of Wick-type stochastic fractional 2D KdV equations

Hossam A. Ghany, Abd-Allah Hyder
Chin. Phys. B, 2014, 23 (**6**): 060503. DOI: 10.1088/1674-1056/23/6/060503

SPECIAL TOPIC — Interdisciplinary physics: Complex network dynamics and emerging technologies

Transient transition behaviors of fractional-order simplest chaotic circuit with bi-stable locally-active memristor and its ARM-based implementation

Zong-Li Yang(杨宗立)[1], Dong Liang(梁栋)[1,2,†], Da-Wei Ding(丁大为)[1,2,‡], Yong-Bing Hu(胡永兵)[1], and Hao Li(李浩)[3]

[1] *School of Electronics and Information Engineering, Anhui University, Hefei* 230601, *China*
[2] *National Engineering Research Center for Agro-Ecological Big Data Analysis & Application, Anhui University, Hefei* 230601, *China*
[3] *State Grid Lu'an Electric Power Supply Company, Lu'an* 237006, *China*

(Received 23 June 2021; revised manuscript received 29 July 2021; accepted manuscript online 22 August 2021)

This paper proposes a fractional-order simplest chaotic system using a bi-stable locally-active memristor. The characteristics of the memristor and transient transition behaviors of the proposed system are analyzed, and this circuit is implemented digitally using ARM-based MCU. Firstly, the mathematical model of the memristor is designed, which is nonvolatile, locally-active and bi-stable. Secondly, the asymptotical stability of the fractional-order memristive chaotic system is investigated and some sufficient conditions of the stability are obtained. Thirdly, complex dynamics of the novel system are analyzed using phase diagram, Lyapunov exponential spectrum, bifurcation diagram, basin of attractor, and coexisting bifurcation, coexisting attractors are observed. All of these results indicate that this simple system contains the abundant dynamic characteristics. Moreover, transient transition behaviors of the system are analyzed, and it is found that the behaviors of transient chaotic and transient period transition alternately occur. Finally, the hardware implementation of the fractional-order bi-stable locally-active memristive chaotic system using ARM-based STM32F750 is carried out to verify the numerical simulation results.

Keywords: fractional calculus, bi-stable locally-active memristor, transient transition behaviors, ARM implementation

PACS: 05.45.–a, 45.10.Hj, 47.10.Fg **DOI:** 10.1088/1674-1056/ac1fdf

1. Introduction

Chua has predicted that there is the fourth fundamental circuit element called memristor, which describes the relation between charge q and magnetic flux ϕ.[1] In 2008, HP (Hewlett Packard) Laboratory first fabricated a practical memristor physical device.[2] From then on, the research of the memristor received widespread attention in many fields of academia and industry. Due to its nonlinear and nonvolatile characteristics, memristors can be applied in many scenarios, such as neural networks,[3–5] memory storage,[6–8] chaotic circuit design[9–11] and secure communications.[12–14]

Researches show that the memristor has many types, and current popular memristors contain the HP memristors,[15–17] piecewise nonlinear memristors,[18–20] continuous nonlinear function memristors,[21–23] locally-active memristors,[24–26] and so on. Recently, the research of locally-active memristors has attracted wide attention because it has the capability of a nonlinear dynamical system to amplify infinitesimal energy fluctuations.[27–29] According to the principle of energy conservation, if a nonlinear dynamical system can produce and maintain oscillations, a locally-active element is essential. Oscillations occur only in locally-active regions.[30] As a novel memory device, the locally-active memristor is first proposed by Chua,[31] and it is considered to be the origin of complexity.[32] Chua proposed a corsage memristor with one pinched hysteresis loop and locally-active ranges, which was analyzed from complex frequency domain.[33] Oscillation of the circuit on the corsage memristor was analyzed via an application of the theory of local activity, edge of chaos and the Hopf-bifurcation.[34] A novel bi-stable nonvolatile locally-active memristor model was introduced, and the dynamics and periodic oscillation were analyzed using the theory of local activity, pole-zero analysis of admittance functions, Hopf bifurcation and the edge of chaos.[35] Jin *et al.* proposed a novel locally-active memristor based on a voltage-controlled generic memristor, analyzed its characteristics and illustrated the concept of local activity via the DC V–I loci of the memristor and nonvolatile memory via the power-off plot of the memristor.[36] Ying *et al.* proposed a nonvolatile locally-active memristor, and the edge of chaos was observed using the method of the small-signal equivalent circuit.[37] Wang *et al.* proposed a locally-active memristor with two pinched hysteresis loops and four locally-active regions, and the effect of locally-active memristors on the complexity of systems was

†Corresponding author. E-mail: 07115@ahu.edu.cn
‡Corresponding author. E-mail: dwding@ahu.edu.cn

discussed.[38]

Fractional calculus is a generalization of the integer-order calculus, and it has the same historical memory characteristic as memristor with respect to time, therefore memristor and memristive system can be extended to fractional-order. Ivo Petráš *et al*. firstly proposed the conception of the fractional-order memristor.[39] Yu *et al*. demonstrated that fractional-order system can describe memory effect better than integer order system in frequency domain.[40] Fouda *et al*. discussed the response of the fractional-order memristor under the DC and periodic signals.[41] A fractional-order HP TiO_2 memristor model was proposed, and the fingerprint analysis of the new model under periodic external excitation was made.[42] Wang *et al*. studied the properties of a fractional-order memristor, and the influences of parameters were analyzed and compared. Then the current–voltage characteristics of a simple series circuit that is composed of a fractional-order memristor and a capacitor were studied.[43]

Nowadays, there are many researches on locally-active memristor.[44–47] Fractional-order locally-active systems can generate more complex dynamic behaviors. However, there are few researches on the nonlinear characteristics of fractional-order locally-active memristor. Our objective is to propose a novel fractional-order continuous nonlinear bi-stable locally-active memristor model, and study its nonlinear characteristics and conclude that the fractional-order memristor is a bi-stable locally-active memristor in certain conditions. Then, we analyze the features of the fractional-order locally-active memristor by time domain waveforms and pinched hysteresis loop at different frequencies, different amplitudes and different orders. In order to verify that the fractional-order memristor is locally-active, we design a fractional-order simplest circuit system using the designed memristor, a linear passive inductor and a linear passive capacitor in series. It is observed that the circuit can produce oscillation and its dynamical behavior is abundant. Particularly, the fractional-order simplest nonlinear circuit using bi-stable locally-active memristor exhibits discontinuous coexisting phenomenon and rich transient transition phenomenon. Moreover, in order to verify the correctness of the theoretical analysis and numerical simulation, the fractional-order simplest chaotic system is implemented by ARM-based MCU. The contributions of this paper are listed as follows: (1) We design and analyze a fractional-order bi-stable locally-active memristor. (2) We build a fractional-order chaotic system based on the proposed memristor and discover its discontinuous coexisting dynamical behaviors and transient transition behaviors. (3) The proposed memristor and chaotic system are implemented digitally by ARM-based hardware.

The structure of this paper is organized as follows: Section 2 introduces the mathematical model of the fractional-order bi-stable locally-active memristor and the power-off plot (POP) and DC V–I loci are used to verify the nonvolatile and the locally-active characteristics. In Section 3, a fractional-order nonlinear circuit using the proposed memristor is established, and the stability of the system is discussed. In Section 4, the nonlinear dynamics and transient transition behaviors of this system are revealed numerically using bifurcation diagrams, Lyapunov exponent spectrum, and phase portraits and so on. In Section 5, the circuit implement is carried out by ARM-based MCU in order to verify the validity of the numerical simulation results. Finally, some concluding remarks are given in the last short section.

2. Preliminaries

In this section, the mathematical definition of the Caputo fractional derivatives and Adomian decoposition method are introduced.

2.1. Fractional calculus

Definition 1[48] The Caputo fractional derivation definition of fractional-order α is

$$J^{\alpha}f(t)=\begin{cases}\dfrac{1}{\Gamma(\alpha)}\int_0^t(t-\tau)^{\alpha-1}f(\tau)\,\mathrm{d}\tau, & \alpha>0,\ t>0,\\ \dfrac{\mathrm{d}^m}{\mathrm{d}t^m}f(t), & \alpha=m,\end{cases}\tag{1}$$

where $\Gamma(\cdot)$ is the gamma function, and $\alpha\in R$, $m\in Z^+$. When $0<\alpha<1$, $D_t^{\alpha}f(t)=\frac{1}{\Gamma(1-\alpha)}\int_0^t\frac{f'(\tau)}{(t-\tau)^{\alpha}}\,\mathrm{d}\tau$.

Definition 2[49] The Riemann–Liouville fractional integral operator of order $\alpha\geq 0$, for a function $f\in C_{\mu},(\mu\geq -1)$ is defined as

$$J^{\alpha}f(t)=\frac{1}{\Gamma(\alpha)}\int_0^t(t-\tau)^{\alpha-1}f(\tau)\,\mathrm{d}\tau,\quad \alpha>0,\ t>0,\tag{2}$$

where $\Gamma(\alpha)=\int_0^{\infty}\mathrm{e}^{-u}u^{\alpha-1}\,\mathrm{d}u$ is the gamma function.

2.2. Adomian decomposition method

For a fractional-order chaotic system $D_{t_0}^{\alpha}\boldsymbol{x}(\boldsymbol{t})=\boldsymbol{f}(\boldsymbol{x}(\boldsymbol{t}))+\boldsymbol{g}(\boldsymbol{t})$, here $\boldsymbol{x}(\boldsymbol{t})=[x_1(t),x_2(t),\ldots,x_n(t)]^{\mathrm{T}}$ are the state variables of the given function, and $\boldsymbol{g}(\boldsymbol{t})=[g_1,g_2,\ldots,g_n]^{\mathrm{T}}$ are the constants for the autonomous system, and the function $\boldsymbol{f}$ can be divided into linear and nonlinear terms

$$\begin{cases}D_{t_0}^{\alpha}\boldsymbol{x}(t)=L\boldsymbol{x}+N\boldsymbol{x}+\boldsymbol{g}(t),\\ \boldsymbol{x}^{(k)}(t_0^+)=\boldsymbol{b}_k,\quad k=0,1,\ldots,m-1,\\ m\in N,\quad m-1<\alpha<m,\end{cases}\tag{3}$$

where $D_{t_0}^{\alpha}$ represents the Caputo differential operator of order α, L is the linear term, N is the nonlinear term, b_k is the initial value. Applying operator $J_{t_0}^{\alpha}$ to both sides of Eq. (3), we obtain

$$\boldsymbol{x}=J_{t_0}^{\alpha}L\boldsymbol{x}+J_{t_0}^{\alpha}N\boldsymbol{x}+\boldsymbol{\Phi},\tag{4}$$

where $\boldsymbol{\Phi} = \sum_{k=0}^{m-1} \boldsymbol{b}_k \frac{(t-t_0)^k}{k!}$ is the initial condition, and $J_{t_0}^{\alpha}$ is Riemann–Liouville fractional integral operator of order α. According to the principle of ADM, the solution of the system can be expressed as

$$\boldsymbol{x}(t) = \sum_{i=0}^{\infty} \boldsymbol{x}_i = \boldsymbol{F}(\boldsymbol{x}(t_0)). \tag{5}$$

The nonlinear terms can be decomposed as follows:

$$\begin{cases} A_j^i = \dfrac{1}{i!}\left[\dfrac{\mathrm{d}^i}{\mathrm{d}\lambda^i} N(v_j^i(\lambda))\right]_{\lambda=0}, \\ v_j^i(\lambda) = \displaystyle\sum_{k=0}^{i} (\lambda)^k x_j^k, \end{cases} \tag{6}$$

where $i = 0,1,2,\ldots,\infty$, $j = 1,2,\ldots,n$, then the nonlinear terms can be expressed as

$$N\boldsymbol{x} = \sum_{i=0}^{\infty} \boldsymbol{A}^i(\boldsymbol{x}^0, \boldsymbol{x}^1, \ldots, \boldsymbol{x}^i). \tag{7}$$

The solution of Eq. (4) is

$$\boldsymbol{x} = \sum_{i=0}^{\infty} \boldsymbol{x}^i = J_{t_0}^{\alpha} L \sum_{i=0}^{\infty} \boldsymbol{x}^i + J_{t_0}^{\alpha} N \sum_{t_0}^{\infty} \boldsymbol{A}^i + J_{t_0}^{\alpha} \boldsymbol{g} + \boldsymbol{\Phi}, \tag{8}$$

namely,

$$\begin{cases} \boldsymbol{x}^0 = \boldsymbol{\Phi}, \\ \boldsymbol{x}^1 = J_{t_0}^{\alpha} L\boldsymbol{x}^0 + J_{t_0}^{\alpha} \boldsymbol{A}^0(\boldsymbol{x}^0), \\ \boldsymbol{x}^2 = J_{t_0}^{\alpha} L\boldsymbol{x}^1 + J_{t_0}^{\alpha} \boldsymbol{A}^1(\boldsymbol{x}^0, \boldsymbol{x}^1), \\ \qquad\vdots \\ \boldsymbol{x}^i = J_{t_0}^{\alpha} L\boldsymbol{x}^{i-1} + J_{t_0}^{\alpha} \boldsymbol{A}^{i-1}(\boldsymbol{x}^0, \boldsymbol{x}^1, \ldots, \boldsymbol{x}^{i-1}), \\ \qquad\vdots \end{cases} \tag{9}$$

3. Bi-stable locally-active memristor

3.1. Memristor model

Based on Chua's unfolding theorem,[50] a generic current-controlled memristor can be described by

$$v(t) = G(x,t)i(t), \tag{10}$$

$$\frac{\mathrm{d}x}{\mathrm{d}t} = g(x,i,t), \quad \alpha > 0, \tag{11}$$

where v and i are the input and output of the memristor, respectively, x is the state variable, and $g(\cdot)$ and $G(\cdot)$ are functions related to a specific memristor.

A novel generic memristor model is proposed as follows:

$$v(t) = k(2x - cx^3)i(t), \tag{12}$$

$$\frac{\mathrm{d}^{\alpha}x}{\mathrm{d}t^{\alpha}} = ax + bx^3 + i(t), \quad \alpha > 0. \tag{13}$$

Based on Eqs. (12) and (13), when the unfolding parameters are set as $a = 4$, $b = -1$, the POP of Eq. (13) with the arrowheads is shown in Fig. 1. Observing the trajectory of motion of the state variable x, we find that there are three intersections with the x-axis located at $x_1 = -2$, $x_2 = 0$, $x_3 = 2$. The dynamic route identifies that the equilibrium points $-E_1$ and E_1 are asymptotically stable, whereas the equilibrium point E_0 is unstable, and the attraction domains of $-E_1$ and E_1 are $(-\infty, 0)$ and $(0, \infty)$, respectively.

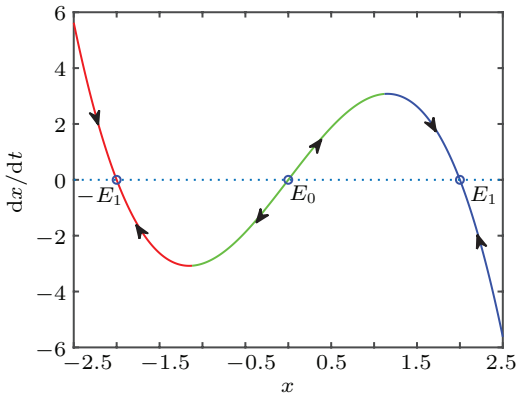

Fig. 1. Power-off plot (POP) of Eq. (13).

3.2. Pinched hysteresis loops

A sinusoidal signal source with amplitude A and frequencies ω is designed to drive the memristor. The dynamical trajectory displays one monostable or bi-stable pinched hysteresis loop as the amplitude A and frequency ω of the sinusoidal signal source take different values.

Let the amplitude $A = 4$ V, $\alpha = 0.9$, and the frequency ω is changed. When $\omega > 3.5$ rad/s, the dynamical trajectory displays double coexisting pinched hysteresis loops as many initial values x_0 are situated on two sides of the origin. Let $x_0 = 1$ and $x_0 = -1$, double coexisting pinched hysteresis loops can be obtained as shown in Figs. 2(a)–2(c). It can be found from Fig. 2 that the double coexisting pinched hysteresis loops of the memristor are located in at least three quadrants. For $\omega > 35$ rad/s, although the dynamical trajectory displays double coexisting pinched hysteresis loops, the memristor is non-active.

Let the frequency $\omega = 6$ rad/s, $\alpha = 0.9$, and the amplitude A is changed. When $A < 6.4$ V, the dynamical trajectory displays one bi-stable pinched hysteresis loop as many initial values x_0 are situated on two sides of the origin. Let $x_0 = 1$ and $x_0 = -1$, double coexisting pinched hysteresis loops can be obtained as shown in Figs. 2(d)–2(f). The same conclusion can be obtained as above.

Let the amplitude $A = 5$ V, $\alpha = 0.9$, and the frequency ω is changed. When 1.4 rad/s $\leqslant \omega < 3.5$ rad/s, the pinched hysteresis loops have a pinch-off point. When $0 \leqslant \omega < 1.4$ rad/s, the pinched hysteresis loops have two pinch-off points, and all of the pinched hysteresis loops are symmetric about $i = 0$, the memristor is monostable memristor. The pinched hysteresis loops and corresponding time domain diagram are shown in Figs. 3(a)–3(d).

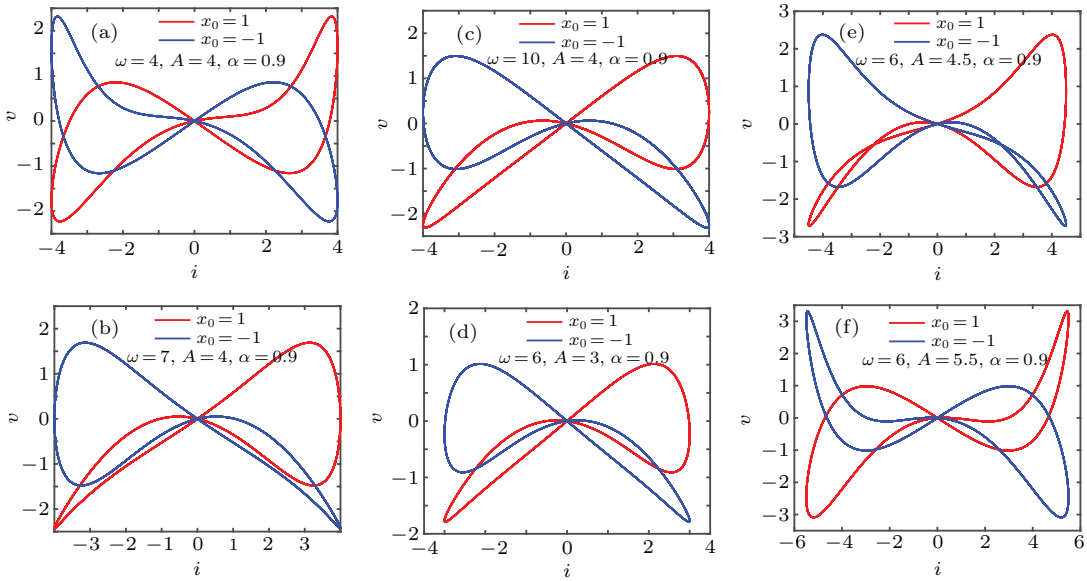

Fig. 2. Double coexisting pinched hysteresis loops when $\alpha = 0.9$, where red curves indicate initial value is $x_0 = 1$, blue curves indicate the initial value is $x_0 = -1$: (a) $A = 4$ V, $\omega = 4$ rad/s, (b) $A = 4$ V, $\omega = 7$ rad/s, (c) $A = 4$ V, $\omega = 10$ rad/s, (d) $A = 3$ V, $\omega = 6$ rad/s, (e) $A = 4.5$ V, $\omega = 6$ rad/s, (f) $A = 5.5$ V, $\omega = 6$ rad/s.

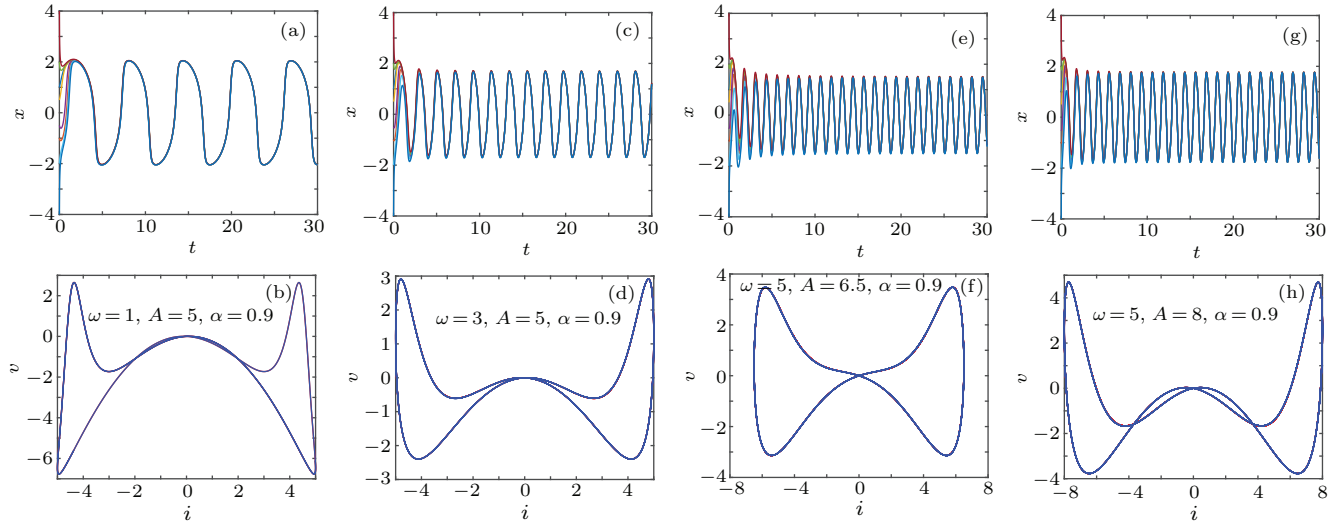

Fig. 3. The time-domain wave and pinched hysteresis loops of monostable memristor: (a) the time-domain diagram when $A = 5$ V, $\omega = 2.1$ rad/s, (b) the pinched hysteresis loops when $A = 5$ V, $\omega = 2.1$ rad/s, (c) the time-domain diagram when $A = 5$ V, $\omega = 1.5$ rad/s, (d) the pinched hysteresis loops when $A = 5$ V, $\omega = 1.5$ rad/s, (e) the time-domain diagram when $A = 6.7$ V, $\omega = 3$ rad/s, (f) the pinched hysteresis loops when $A = 6.7$ V, $\omega = 3$ rad/s, (g) the time-domain diagram when $A = 8$ V, $\omega = 3$ rad/s, (h) the pinched hysteresis loops when $A = 8$ V, $\omega = 3$ rad/s.

In the same way, let the frequency $\omega = 5$ rad/s, and the amplitude A is changed. When $A > 6$ V, the pinched hysteresis loops have one pinch-off point. When $6.85\ \text{V} \leqslant A < 10.5$ V, the pinched hysteresis loop has two pinch-off points, and all of the pinched hysteresis loops are symmetric about $i = 0$, the memristor is monostable memristor. The pinched hysteresis loops and corresponding time domain diagram are shown in Figs. 3(e)–3(h).

Let the amplitude $A = 4$ V, $\omega = 5$ rad/s, and the order α is changed. When $0.787 \leqslant \alpha < 1$, the pinched hysteresis loop has two pinch-off points. With the order α increasing, the non-origin pinch-off point moves from left to right until it disappears. When $\alpha < 0.787$, the pinched hysteresis loop has a pinch-off point of the origin, and it is symmetric about $i = 0$. The pinched hysteresis loops are shown in Fig. 4.

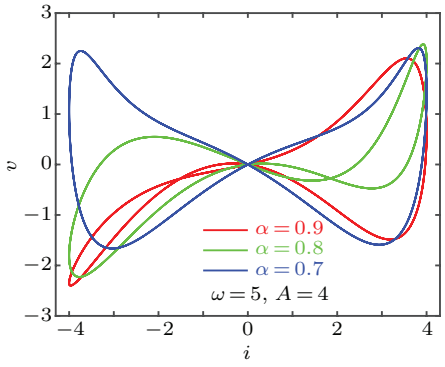

Fig. 4. The pinched hysteresis loops when $A = 4$, $\omega = 5$, where red curve indicates the order of $\alpha = 0.9$, green curve indicates the order of $\alpha = 0.8$, blue curve indicates the order of $\alpha = 0.7$.

3.3. DC V–I plots

DC V–I plot is the Ohm's law of the memristor, which can clearly show the intrinsic features of the memristor. Let $x = X$, $\mathrm{d}x/\mathrm{d}t|_{x=X} = 0$, Eq. (13) can be described as follow:

$$4X - X^3 + I = 0. \tag{14}$$

Solving Eq. (14) for the equilibrium point (X, I), a function between the state X and the applied DC current I can be derived, and we have

$$X = \widehat{X}(I). \tag{15}$$

Then setting $k = 1$ and substituting Eq. (15) into Eq. (12), the DC voltage V can be calculated as

$$V = \widehat{V}(I) = (4X - cX^3)I. \tag{16}$$

Based on Eqs. (15) and (16), when the parameter c is set as 0.4, the DC X–I and V–I plots of the memristor can be obtained, as shown in Figs. 5(a) and 5(b), respectively. When the parameter c is set as different values, the DC V–I plots are drawn as shown in Figs. 5(c) and 5(d). It can be seen from Fig. 5 that the slopes of three parts of the DC V–I curves are negative, hence the designed memristor is locally active.

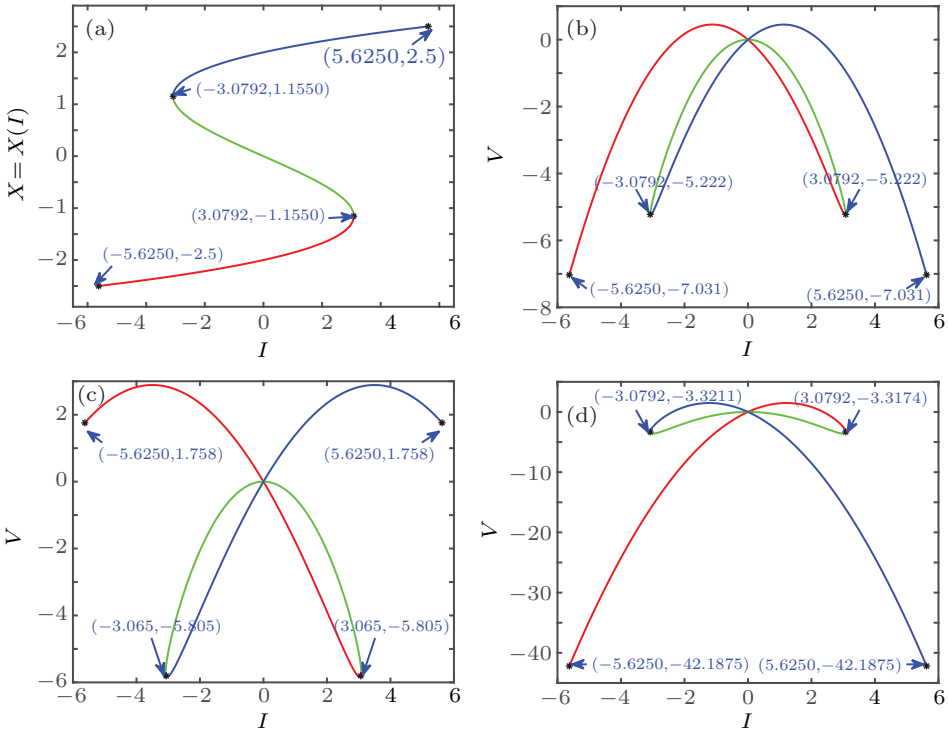

Fig. 5. DC X–I and V–I loci. (a) The equilibrium state curve on the X–I plane for the DC current on interval -6 A$< I <$ 6 A, (b) DC V–I plot when $c = 0.4$, (c) DC V–I plot when $c = 0.3$, (d) DC V–I plot when $c = 0.8$.

4. Fractional-order bi-stable memristive system

The well-known simplest chaotic system was presented by Chua.[51] The system contains three circuit elements, a resistance, an inductance and a memristor. When the memristor is replaced by a bi-stable locally-active memristor, a novel 3D autonomous fractional-order memristive chaotic system is given by

$$\begin{aligned} \frac{\mathrm{d}^\alpha x}{\mathrm{d}t^\alpha} &= y/C, \\ \frac{\mathrm{d}^\alpha y}{\mathrm{d}t^\alpha} &= -[x + ky(2z - cz^3)]/L, \\ \frac{\mathrm{d}^\alpha z}{\mathrm{d}t^\alpha} &= az + bz^3 - y. \end{aligned} \tag{17}$$

The parameter values are $C = 1$, $L = 1$, $a = 4$, $b = -1$. The state variables in terms of circuit variables are $x(t) = v_C(t)$ (voltage across capacitor C), $y(t) = i_L(t)$ (current through inductor L) and $z(t)$ is the internal state of the bi-stable locally-active memristor.

From basic circuit theory, it is not possible to have an oscillation with three independent state variables if we use the non-active memristor. However, if we use a bi-stable locally-active memristor in the circuit, the autonomous system can generate oscillation.

4.1. The stability of the equilibria

To evaluate the equilibrium points, let

$$\begin{aligned} \frac{\mathrm{d}^\alpha x}{\mathrm{d}t^\alpha} &= 0, \\ \frac{\mathrm{d}^\alpha y}{\mathrm{d}t^\alpha} &= 0, \end{aligned}$$

$$\frac{\mathrm{d}^{\alpha}z}{\mathrm{d}t^{\alpha}}=0. \tag{18}$$

Then $(x^{\mathrm{eq}},y^{\mathrm{eq}},z^{\mathrm{eq}})=(0,0,0),(0,0,2),(0,0,-2)$ are the equilibrium. The Jacobian matrix of system (16) at $(x^{\mathrm{eq}},\ y^{\mathrm{eq}},\ z^{\mathrm{eq}})=(0,0,z^{*})$ is

$$\boldsymbol{J}_{\mathrm{E}}=\begin{pmatrix}0 & 1 & 0\\ -1 & -k(z^{*}-cz^{*3}) & 0\\ 0 & -1 & 4-3z^{*}\end{pmatrix}. \tag{19}$$

The characteristic equation of the Jacobian matrix (19) is described as follows:

$$(\lambda-4+3z^{*2})[\lambda^{2}+\lambda k(2z^{*}-cz^{*3})+1]=0. \tag{20}$$

Lemma 1[52] The fractional-order nonlinear system

$$D^{\alpha}\boldsymbol{X}=\boldsymbol{f}(\boldsymbol{X}),\quad 0<\alpha\leqslant 1 \tag{21}$$

is asymptotically stable at the equilibrium $(x^{\mathrm{eq}},\ y^{\mathrm{eq}},\ z^{\mathrm{eq}})$, if all eigenvalues satisfy the condition

$$|\arg(\lambda)|>\frac{\alpha\pi}{2}, \tag{22}$$

where $\boldsymbol{X}=(x,y,z)^{\mathrm{T}}$, $\boldsymbol{f}(\boldsymbol{X})=(f_1(\boldsymbol{X}),f_2(\boldsymbol{X}),f_3(\boldsymbol{X}))^{\mathrm{T}}$, and $\arg(\lambda)$ is the principal argument of eigenvalue λ.

Obviously, Eq. (20) has a real solution $\lambda_1=4-3z^{*2}$. To analyze the stability of the equilibrium points, the characteristic roots of Eq. (20) are discussed as follows:

When the equilibrium point is the origin, $\lambda_1=4$, $\lambda_2=\mathrm{i}$, $\lambda_3=-\mathrm{i}$. Obviously, there are no negative real parts in Eq. (20), therefore the origin is unstable.

When the equilibrium point is $(x^{\mathrm{eq}},\ y^{\mathrm{eq}},\ z^{\mathrm{eq}})=(0,\ 0,\ 2)$, $(0,\ 0,\ -2)$, $\lambda_1=-8$, $\lambda_{2,3}=\frac{-k(2z^{*}-cz^{*3})\pm\sqrt{k(2z^{*}-cz^{*3})-4}}{2}$.

If λ_2 and λ_3 are real values, the inequality $(k(2z^{*}-cz^{*3}))^{2}-4\geqslant 0$ holds, namely, $k(2z^{*}-cz^{*3})\geqslant 2$ or $k(2z^{*}-cz^{*3})\leqslant -2$.

When $k(2z^{*}-cz^{*3})\geqslant 2$, then $\lambda_2<0$, $\lambda_3<0$. In this case the equilibrium point is asymptotically stable. For the equilibrium (0, 0, 2), if $c<0.5$, then $k\geqslant\frac{1}{2-4c}$. If $c>0.5$, then $k\leqslant\frac{1}{2-4c}$. They are shown in region III of Fig. 6. For the equilibrium (0, 0, −2), if $c>0.5$, then $k\geqslant\frac{-1}{2-4c}$. If $c<0.5$, then $k\leqslant\frac{-1}{2-4c}$. They are shown in region IV of Fig. 6.

When $k(2z^{*}-cz^{*3})\leqslant -2$, then $\lambda_2>0$, $\lambda_3>0$. In this case the equilibrium point is unstable. For the equilibrium (0, 0, 2), if $c>0.5$, then $k\geqslant\frac{-1}{2-4c}$. If $c<0.5$, then $k\leqslant\frac{-1}{2-4c}$. They are shown in region IV of Fig. 6. For the equilibrium (0, 0, −2), if $c<0.5$, then $k\geqslant\frac{1}{2-4c}$. If $c>0.5$, then $k\leqslant\frac{1}{2-4c}$. They are shown in region III of Fig. 6.

If λ_2 and λ_3 are the complex roots, the inequality $(k(2z^{*}-cz^{*3}))^{2}-4<0$ holds, namely, $-2<k(2z^{*}-cz^{*3})<2$.

As $0<k(2z^{*}-cz^{*3})<2$, λ_2 and λ_3 are the conjugate complex roots with negative real parts $\mathrm{Re}(\lambda_{2,3})=-k(2z^{*}-cz^{*3})<0$. In this case the equilibrium point is asymptotically stable. For the equilibrium (0, 0, 2), if $c<0.5$, then $0<k<\frac{1}{2-4c}$. If $c>0.5$, then $\frac{1}{2-4c}<k<0$. They are shown in region I of Fig. 6. For the equilibrium (0, 0, −2), if $c>0.5$, then $0<k<\frac{-1}{2-4c}$. If $c<0.5$, then $\frac{-1}{2-4c}<k<0$. They are shown in region II of Fig. 6.

As $-2<k(2z^{*}-cz^{*3})<0$, λ_2 and λ_3 are the conjugate complex roots with positive real parts $\mathrm{Re}(\lambda_{2,3})=-k(2z^{*}-cz^{*3})>0$. In this case the equilibrium point is unstable. For the equilibrium (0, 0, 2), if $c>0.5$, then $0<k<\frac{-1}{2-4c}$. If $c<0.5$, then $\frac{-1}{2-4c}<k<0$. They are shown in region II of Fig. 6. For the equilibrium (0, 0, −2), if $c<0.5$, then $0<k<\frac{1}{2-4c}$. If $c>0.5$, then $\frac{1}{2-4c}<k<0$. They are shown in region I of Fig. 6.

The asymptotically stable regions and unstable regions in the k–c plane are separated by the curves of $k(2z^{*}-cz^{*3})=2$ and $k(2z^{*}-cz^{*3})=-2$, which are shown as the red curves and blue curves in Fig. 6, respectively.

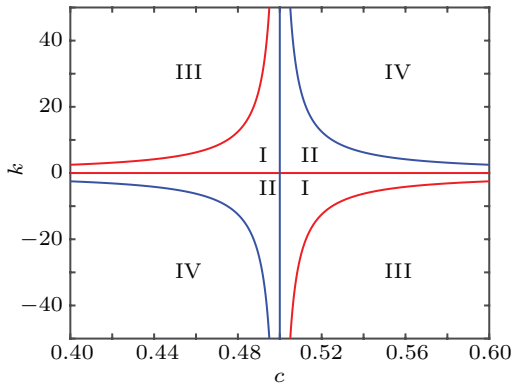

Fig. 6. Asymptotically stable and unstable regions of the system (16) in the k–c plane.

4.2. Solution of the fractional-order bi-stable simplest memristive system

According to the properties of the fractional integral operator, we suppose that the initial values of the system (17) are (x_0,y_0,z_0), and apply Riemann–Liouville operator $J_{t_0}^{\alpha}$ to both sides of Eq. (17), we obtain

$$\begin{aligned}x&=J_{t_0}^{\alpha}y+x_0,\\ y&=-J_{t_0}^{\alpha}x-2kJ_{t_0}^{\alpha}yz+kcJ_{t_0}^{\alpha}yz^{3}+y_0,\\ z&=J_{t_0}^{\alpha}(4z-y)-J_{t_0}^{\alpha}z^{3}+z_0.\end{aligned} \tag{23}$$

Based on ADM method,[53] considered the calculation of the computer and the precision of the solution, the first five ADM polynomial of nonlinear terms $-yz$, yz^3 and $-z^3$ are decomposed as follow:

$$\begin{aligned}A_{21}^{0}&=-y_0z_0,\\ A_{21}^{1}&=-y_1z_0-y_0z_1,\\ A_{21}^{2}&=-y_2z_0-y_1z_1-y_0z_2,\\ A_{21}^{3}&=-y_3z_0-y_2z_1-y_2z_2-y_0z_3,\\ A_{21}^{4}&=-y_4z_0-y_3z_1-y_1z_3-y_2z_2-y_0z_4,\end{aligned} \tag{24}$$

$$
\begin{aligned}
A_{22}^0 &= y_0(z_0)^3,\\
A_{22}^1 &= y_1(z_0)^3+3y_0z_1(z_0)^2,\\
A_{22}^2 &= 3y_0(z_0)^2z_2+3y_0z_0(z_1)^2+3y_1(z_0)^2z_1+y_2(z_0)^3,\\
A_{22}^3 &= 3y_0(z_0)^2z_3+3y_1(z_0)^2z_2+3y_2(z_0)^2z_1\\
&\quad +6y_0z_0z_1z_2+3y_1z_0(z_1)^2+y_0(z_1)^3+y_3(z_0)^3,\\
A_{22}^4 &= 3y_0(z_0)^2z_4+3y_1(z_0)^2z_3+3y_2(z_0)^2z_2+3y_3(z_0)^2z_1\\
&\quad +6y_0z_0z_1z_3+6y_1z_0z_1z_2+3y_2z_0(z_1)^2\\
&\quad +3y_0z_0(z_2)^2+3y_0(z_1)^2z_2+y_1(z_1)^3+y_4(z_0)^3, \qquad (25)\\
A_3^0 &= -(z_0)^3,\\
A_3^1 &= -3(z_0)^2z_1,\\
A_3^2 &= -3(z_0)^2z_2-3z_0(z_1)^2,\\
A_3^3 &= -3(z_0)^2z_3-6z_0z_1z_2-(z_1)^3,\\
A_3^4 &= -3(z_0)^2z_4-6z_0z_1z_3-3z_0(z_2)^2-2(z_1)^2z_2. \qquad (26)
\end{aligned}
$$

Therefore, we can obtain

$$
\begin{aligned}
-yz &= A_{21}^0+A_{21}^1+\cdots\\
&= (-y_0z_0)+(-y_1z_0-y_0z_1)+\cdots, \qquad (27)\\
yz^3 &= A_{22}^0+A_{22}^1+\cdots\\
&= [y_0(z_0)^3]+[y_1(z_0)^3+3y_0z_1(z_0)^2]+\cdots, \qquad (28)\\
-z^3 &= A_3^0+A_3^1+\cdots\\
&= [-(z_0)^3]+[-3(z_0)^2z_1]+\cdots. \qquad (29)
\end{aligned}
$$

Substituting expressions (27)–(29) into Eq. (23), it can be obtained

$$
\begin{aligned}
x &= J_{t_0}^{\alpha}\left(\sum_{v=0}^{i}y_v\right)+x_0,\\
y &= -J_{t_0}^{\alpha}\left(\sum_{v=0}^{i}x_v\right)-2kJ_{t_0}^{\alpha}[(y_0z_0)+(y_1z_0+y_0z_1)+\cdots]\\
&\quad +kcJ_{t_0}^{\alpha}\left\{[y_0(z_0)^3]+[y_1(z_0)^3+3y_0z_1(z_0)^2]+\cdots\right\}+y_0\\
z &= J_{t_0}^{\alpha}\left(4\left(\sum_{v=0}^{i}z_v\right)-\left(\sum_{v=0}^{i}y_v\right)\right)\\
&\quad -J_{t_0}^{\alpha}\left\{[(z_0)^3]+[3(z_0)^2z_1]+\cdots\right\}+z_0. \qquad (30)
\end{aligned}
$$

Therefore, the discrete iterative formula of the system (17) is described as

$$
\begin{aligned}
x_{m+1} &= x_m+y_m\frac{h^{\alpha}}{\Gamma(\alpha+1)}\\
&\quad +[-x_m-2ky_mz_m+kcy_m(z_m)^3]\frac{h^{2\alpha}}{\Gamma(2\alpha+1)}+\cdots,\\
y_{m+1} &= y_m+[-x_m-2ky_mz_m+kcy_m(z_m)^3]\frac{h^{\alpha}}{\Gamma(\alpha+1)}\\
&\quad +[-y_m-2ky_mz_m+kcy_m(z_m)^3+\cdots]\frac{h^{2\alpha}}{\Gamma(2\alpha+1)}+\cdots,\\
z_{m+1} &= z_m+[4z_m-y_m-(z_m)^3]\frac{h^{\alpha}}{\Gamma(\alpha+1)}\\
&\quad +[4z_m-(-x_m-2ky_mz_m+kcy_m(z_m)^3)+\cdots]\\
&\quad \times\frac{h^{2\alpha}}{\Gamma(2\alpha+1)}+\cdots, \qquad (31)
\end{aligned}
$$

where h is the iteration step size. The iteration algorithm for the simulation calculations is expressed as follows:

$$
\begin{aligned}
C_{10} &= x_m,\\
C_{20} &= y_m,\\
C_{30} &= z_m, \qquad (32)\\
C_{11} &= C_{20},\\
C_{21} &= -C_{10}-2kC_{20}C_{30}+kcC_{20}(C_{30})^3,\\
C_{31} &= 4C_{30}-C_{20}-(C_{30})^3, \qquad (33)\\
C_{12} &= C_{21},\\
C_{22} &= -C_{11}-2k(C_{21}C_{30}+C_{20}C_{31})\\
&\quad +kc(C_{21}(C_{30})^3+3C_{20}C_{31}(C_{30})^2),\\
C_{32} &= 4C_{31}-C_{21}-3(C_{30})^2C_{31}, \qquad (34)\\
C_{13} &= C_{22},\\
C_{23} &= -C_{12}-2k(C_{22}C_{30}+C_{20}C_{32}+C_{21}C_{31}\frac{\Gamma(2\alpha+1)}{\Gamma^2(\alpha+1)})\\
&\quad +kc(3C_{20}(C_{30})^2C_{32}+3C_{20}C_{30}(C_{31})^2\\
&\quad +3C_{21}C_{31}(C_{30})^2+C_{22}(C_{30})^3),\\
C_{33} &= 4C_{32}-C_{22}-3(C_{30})^2C_{32}-3C_{30}(C_{31})^2, \qquad (35)\\
C_{14} &= C_{23},\\
C_{24} &= -C_{13}-2k(C_{23}C_{30}+C_{20}C_{33}\\
&\quad +C_{22}C_{31}\frac{\Gamma(3\alpha+1)}{\Gamma(\alpha+1)\Gamma(2\alpha+1)}\\
&\quad +C_{22}C_{32}\frac{\Gamma(4\alpha+1)}{\Gamma^2(2\alpha+1)})\\
&\quad +kc(3C_{20}(C_{30})^2C_{33}+3C_{21}C_{32}(C_{30})^2\\
&\quad +3C_{22}C_{31}(C_{30})^2,+6C_{20}C_{30}C_{31}C_{32}\\
&\quad +3C_{21}C_{30}(C_{31})^2+C_{20}(C_{31})^3+C_{23}(C_{30})^3),\\
C_{34} &= 4C_{33}-C_{23}-3(C_{30})^2C_{33}\\
&\quad -6C_{30}C_{31}C_{32}-(C_{31})^3\frac{\Gamma(3\alpha+1)}{\Gamma^3(\alpha+1)}, \qquad (36)\\
C_{15} &= C_{24},\\
C_{25} &= -C_{14}-2k(C_{24}C_{30}+C_{20}C_{34}\\
&\quad +(C_{23}C_{31}+C_{21}C_{33})\frac{\Gamma(4\alpha+1)}{\Gamma(\alpha+1)\Gamma(3\alpha+1)}\\
&\quad +C_{22}C_{32}\frac{\Gamma(4\alpha+1)}{\Gamma^2(2\alpha+1)})\\
&\quad +kc(3C_{20}(C_{30})^2C_{34}+3C_{21}C_{33}(C_{30})^2\\
&\quad +3C_{22}C_{32}(C_{30})^2+3C_{23}C_{31}(C_{30})^2\\
&\quad +6C_{20}C_{30}C_{31}C_{33}+6C_{21}C_{30}C_{31}C_{32}\\
&\quad +3C_{22}C_{30}(C_{31})^2+3C_{20}C_{30}(C_{32})^2+3C_{20}C_{32}(C_{31})^2\\
&\quad +C_{21}(C_{31})^3\frac{\Gamma(4\alpha+1)}{\Gamma^4(\alpha+1)}+C_{24}(C_{30})^3),\\
C_{35} &= 4C_{34}-C_{24}-3(C_{30})^2C_{34}-6C_{30}C_{31}C_{34}-3C_{30}(C_{32})^2
\end{aligned}
$$

$$-3(C_{31})^3 C_{32}\frac{\Gamma(4\alpha+1)}{\Gamma^2(\alpha+1)\Gamma(2\alpha+1)}. \quad (37)$$

According to Eqs. (32)–(37), we can obtain the solutions of the proposed system, then analyze the dynamical characteristics of the system.

4.3. Analysis of complex dynamical behaviors

Coexisting phase diagrams, coexisting bifurcation diagrams, basins of attractor and coexisting Lyapunov exponents are applied to analyze the dynamical behaviors of system (17).

4.3.1. Bifurcation analysis and Lyapunov exponents

4.3.1.1. Two-parameter bifurcation

In order to show parameter-related dynamical behaviors of the proposed system, a two-parameter bifurcation diagram should first be computed. We know that there is a fractional-order bi-stable memristor used in system (17), when $a = 4$, $c = 0.5$, $\alpha = 0.8$, two examples of two-parameter bifurcation diagrams for different initial conditions $(x_0, y_0, z_0) = (1, 1, 1)$ and $(x_0, y_0, z_0) = (-1, -1, -1)$ are shown in Figs. 7(a) and 7(b), respectively. The regions marked with different colors represent different attractor types and the navy blue regions imply the orbit tending to infinite. In addition, for different parameters, many classes of attractors cannot be completely distinguished, such as limit cycles with different periodicity and chaotic attractors with different topologies. The two-parameter bifurcation diagrams show rich dynamical behaviors and coexisting phenomenon in our system.

In Fig. 7(a), there are many regions marked with different colors, corresponding to the four different attractor types (navy blue region indicates the attractor tending to infinite), namely, cyan area, light area and yellow area indicate point attractor, limit cycle and chaos, respectively. Comparing Fig. 7(b) with Fig. 7(a), it is easily seen that the two-parameter bifurcation diagram from system (17) is almost completely asymmetric.

As shown in Fig. 7(c), there are three different attractor types, which are marked by three different colors, namely, the blue area indicates point attractors, light blue area indicates period attractors and the yellow area indicates chaotic attractors. In contrast, the period attractors have very small area marked by light blue, and the point attractors have biggest area marked by blue. In Fig. 7(d), there are three regions marked with different colors, corresponding to the three different attractor types. The blue area indicates point attractors, the light blue area indicates period attractors, and the yellow area indicates chaotic attractors. From Fig. 7, stable point, periodic and chaotic areas can be easily identified.

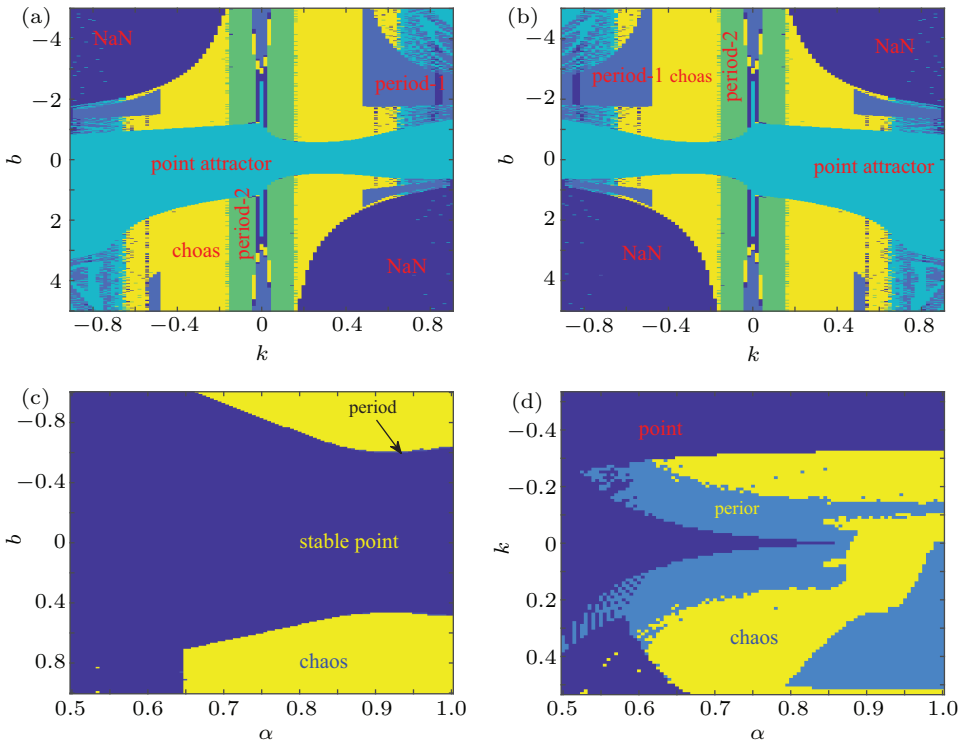

Fig. 7. Two-parameter bifurcation diagrams (a) in k–b plane for initial value (1, 1, 1), (b) in k–b plane for initial value (−1, −1, −1), (c) in α–b plane for initial value (1, 1, 1), (d) in $\alpha - k$ plane for initial value (1, 1, 1).

4.3.1.2. Coexisting bifurcation

Lyapunov exponents are considered as one of the most useful diagnostic tools for analyzing dynamical behaviors of nonlinear system, and coexisting bifurcation analysis can compare the characteristics of a nonlinear system in different initial values. The method of Ref. [54] is used to solve the Lyapunov exponents in this paper. Based on the two-parameter bifurcation diagram, we can trace the dynamics to compute a

single-parameter bifurcation diagram, i.e., $b = 1.5$, $b = -1.5$ and $k = 0.5$, $k = -0.5$. We choose two sets of different initial values (1, 1, 1) and $(-1, -1, -1)$, and plot coexisting bifurcation diagrams of x versus b, x versus k and z versus α. The corresponding bifurcation diagrams and Lyapunov exponents are shown in Figs. 8–10, respectively.

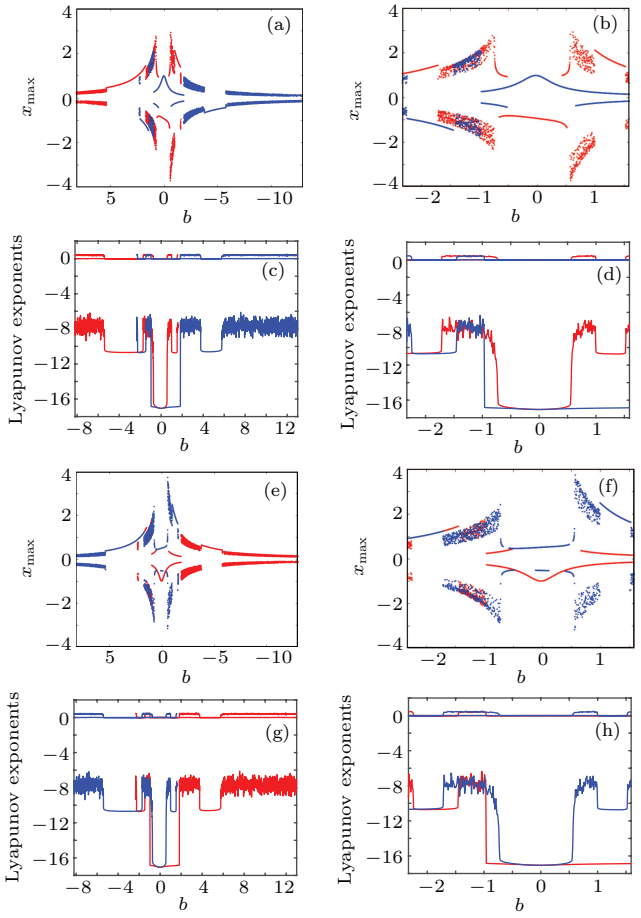

Fig. 8. Bifurcation diagrams with respect to x and Lyapunov exponents. (a) $k = 0.5$, x_{max} excited by two sets of initial value (1,1,1) (red) and initial value $(-1, -1, -1)$ (blue), (b) $k = 0.5$, coexisting bifurcation of x_{max} for initial value (1, 1, 1) (red) and initial value $(-1, -1, -1)$ (blue), (c) $k = 0.5$, Lyapunov exponents corresponding to (a), (d) $k = 0.5$, coexisting Lyapunov exponents corresponding to (b), (e) $k = -0.5$, x_{max} excited by two sets of initial value (1, 1, 1) (red) and initial value $(-1, -1, -1)$ (blue), (f) $k = -0.5$, coexisting bifurcation of x_{max} for initial value (1, 1, 1) (red) and initial value $(-1, -1, -1)$ (blue), (g) $k = -0.5$, Lyapunov exponents corresponding to (e), (h) $k = -0.5$, coexisting Lyapunov exponents corresponding to (f).

It is found from Fig. 8 that system (17) occurs alternately the phenomenon of period and chaos with the increase of parameter. When $k = 0.5$, $b \in [-8.2, -2.33]$, system (17) produces chaotic oscillation and period oscillation only in initial value (1, 1, 1). When $k = 0.5$, $b \in [-2.34, 1.59]$, system (17) undergoes coexisting chaos and period-1 states, coexisting point attractor and period-1 states, coexisting point attractor and chaos states. When $k = 0.5$, $b \in [1.6, 13]$, the coexisting oscillation disappears and system (17) alternately occurs period and chaos oscillation only in initial value $(-1, -1, -1)$. When $k = -0.5$, $b \in [-8.2, 13]$, system (17) undergoes almost the same process as $k = 0.5$, shown in Figs. 8(a), 8(b), 8(e), and 8(f). Symmetry reflects the beauty of harmony and unity. In general, if a system manifests a symmetric transformation $T : (x, y, z) \to (-x, -y, -z)$, it can be found that the system is invariant under T, and emerges dynamic behaviors in pairs. In contrast, our system does not satisfy the condition of a symmetric transformation T, we still find that the bifurcation plots are not perfectly symmetrical with respect to b-axis, x_{max}-axis and center. This indicates that system (17) with the proposed bi-stable locally-active memristor possesses the unique characteristics. The corresponding Lyapunov exponents are shown in Figs. 8(c), 8(d), 8(g), and 8(h).

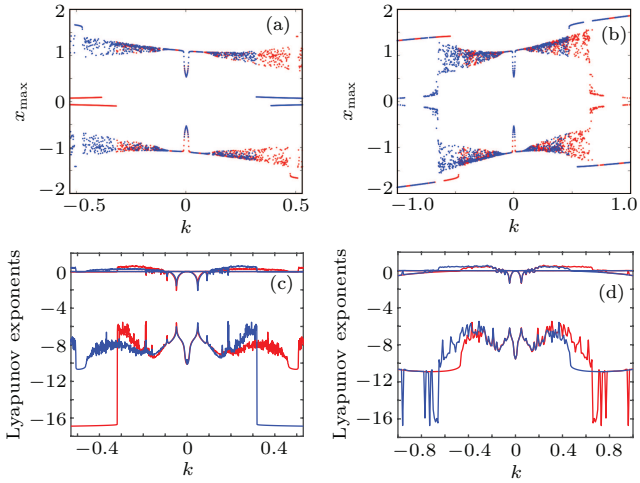

Fig. 9. Coexisting bifurcation diagrams with respect to x and Lyapunov exponents. (a) $b = 1.5$, coexisting bifurcation of x_{max} for initial value (1,1,1) (red) and initial value $(-1, -1, -1)$ (blue), (b) $b = -1.5$, coexisting bifurcation of x_{max} for initial value (1, 1, 1) (red) and initial value $(-1, -1, -1)$ (blue), (c) $b = 1.5$, Lyapunov exponents corresponding to (a), (d) $b = -1.5$, coexisting Lyapunov exponents corresponding to (b).

It is found from Fig. 9 that with the increase of parameter k, system (17) alternately occurs the phenomenon of periods and chaos. When $b = 1.5$, $k \in [-4, -0.5329]$, system (17) produces a stable point attractor only in initial value (1,1,1). When $b = 1.5$, $k \in [-0.5328, -0.3]$, system (17) undergoes coexisting chaos and point attractor states, coexisting period-1 and point attractor states, when $k \in [-0.3, 0.3]$, the coexisting phenomenon disappears and system (17) undergoes chaos to period to chaos. When $k \in [0.3, 0.5328]$, the coexisting phenomenon appears again, and system (17) undergoes a symmetrical process with $k \in [-0.5328, -0.3]$. When $b = 1.5$, $k \in [0.5329, 4]$, system (17) produces stable point attractor only in initial value $(-1, -1, -1)$. When $b = -1.5$, $k \in [-0.5328, 0.5328]$, system (17) undergoes coexisting chaos and point attractor states. When $k \in [-4, -0.5328] \cup k \in [0.5328, 4]$, the coexisting phenomenon disappears and system (17) only appears stable point attractor. We find that the bifurcation plots are not perfectly symmetrical with respect to k-axis, x_{max}-axis and center. The corresponding Lyapunov exponents are shown in Figs. 9(c) and 9(d).

It is found from Fig. 10(a) that with the increase of parameter α, system (17) alternately occurs the phenomenon of stable point, periods and chaos. When $b=-1.5$, $k=0.5$, $\alpha\in[0.5,0.63]$, system (17) produces stable point attractor in all values. When $b=-1.5$, $k=0.5$, $\alpha\in(0.63,0.78]$, system (17) produces chaos oscillation in all values. When $b=-1.5$, $k=0.5$, $\alpha\in(0.78,1]$, system (17) undergoes coexisting chaos and period states. The corresponding Lyapunov exponents are shown in Fig. 10(b).

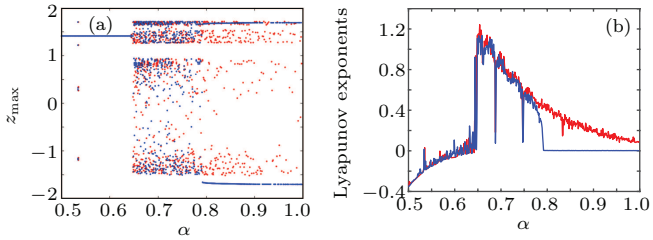

Fig. 10. Coexisting bifurcation diagrams with respect to z versus α and Lyapunov exponents. (a) $k=0.5$, $b=-1.5$, coexisting bifurcation of $z_{\max}$ for initial value (1, 1, 1) (red) and initial value $(-1,-1,-1)$ (blue), (b) $k=0.5$, $b=-1.5$, Lyapunov exponents corresponding to (a).

4.3.2. Coexisting attractors and attraction basins

If a nonlinear system with bi-stable memristor can produce oscillation, it must have coexisting attractors. Based on bifurcation plots in Figs. 7–10, we set parameters $a=4$, $c=0.5$, $\alpha=0.8$, $h=0.001$ and change parameters b and k, then, we can draw phase diagrams as shown in Fig. 11. We find that there are two kinds of chaotic attractors and two kinds of period-I cycles in the system, and called chaotic attractor I and chaotic attractor II, cycle I and cycle II. Figure 11(a) shows the coexistence of cycle I and chaotic attractor I. Figures 11(b) and 11(c) only show cycle I and attractor I, respectively. Figure 11(d) shows the coexistence of attractor I and pointer attractor. Figure 11(e) shows the coexistence of two pointer attractors in the system. Figure 11(f) shows the coexistence of chaotic attractor II and pointer attractor. Figure 11(g) shows the coexistence of cycle II and pointer attractor. Figure 11(h) shows the coexistence of cycle II and pointer attractor. From Fig. 11, we also can see the coexisting phenomenon of system (17) is intermittent.

The different types of attractors coexist stably in the proposed simple chaotic system, their basins of attraction represent the states of the attractors in the initial state space. When we set parameters $a=4$, $c=0.5$, $\alpha=0.8$, $h=0.001$ and change parameters b, we can draw basins of attraction as shown in Fig. 12. In Fig. 12, the basins of attraction of the point and chaos attractors of system (17) are indicated by blue and yellow, respectively. The light blue region indicates the attractor tending to infinite. Comparing Fig. 12(b) with Fig. 12(a), it is easily seen that the basins of attraction from system (17) have similar area shapes when the parameter b is set as 1 and -1.

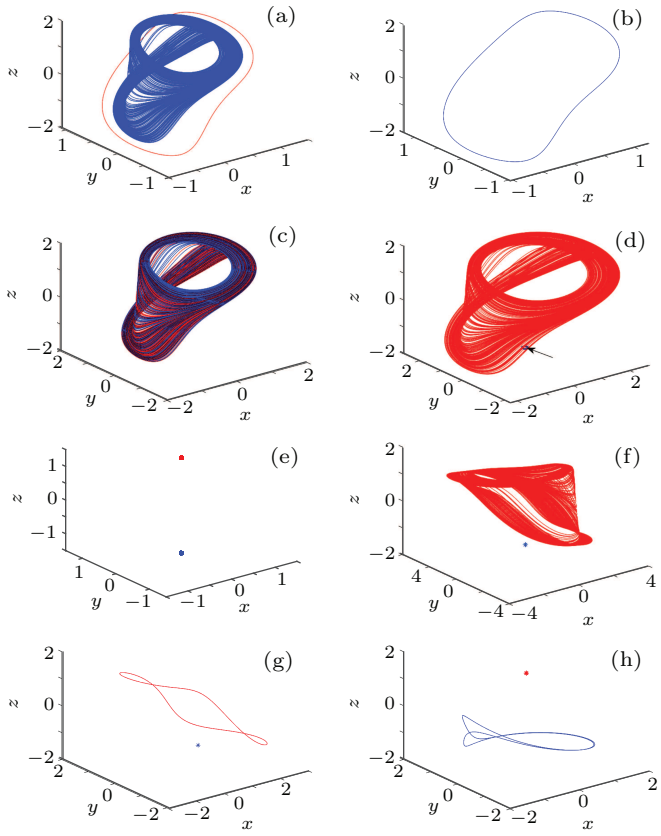

Fig. 11. Coexisting attractor, red curves indicate initial value of (1, 1, 1), blue curves indicate the initial value of $(-1,-1,-1)$; (a) $k=0.5$, $b=-2.33$, (b) $k=0.5$, $b=-2$, (c) $k=0.5$, $b=-1.3$, (d) $k=0.5$, $b=-0.8$, (e) $k=0.5$, $b=0.4$, (f) $k=0.5$, $b=0.6$, (g) $k=0.5$, $b=1.2$, (h) $k=-1.5$, $b=1.15$.

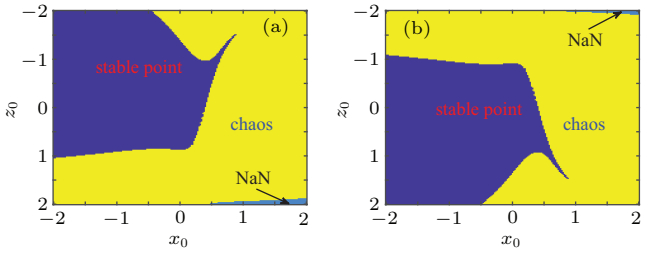

Fig. 12. Attractor basins for (a) $b=1$, (b) $b=-1$.

4.4. Transient transition

Transient chaos and transient period are unique phenomenon in nonlinear systems with locally-active memristor.[55,56] This section will focus on the transient transition behaviors of the proposed system, and study the transient transition phenomena with changing parameters of the system and initial value.

4.4.1. Transient transition when parameter k changes

To research the rich transient behaviors when the parameter k changes, we firstly fix the parameters $\alpha=0.8$, $a=4$, $c=0.5$, $b=1.5$ and initial value (1, 1, 1), then choose the parameter $k\in(0.01,0.51)$.

Setting $k=0.06$, the simulation time $t\in(0,300)$, the time-domain wave and phase diagram of the state variable z

are shown in Figs. 13(a) and 12(b). When $t \in (0,140)$, the time-domain wave is shown in the blue domain of Fig. 13(a), in this time, $LE_1 = 0.0220$, $LE_2 = 0.0073$, $LE_3 = -10.6775$, so the system is chaos. When $t \in (141,165)$, the time-domain wave is shown in the green domain of Fig. 13(a), the system displays an unstable chaotic state. When $t \in (166,300)$, the system displays a period state, which is shown in the red domain of Fig. 13(a). The corresponding phase diagram is shown in Fig. 13(b). When $k = 0.13$, $t \in (0,150)$, the system is chaotic state, which is shown in the blue domain of Fig. 13(c), then $t \in (150,200)$, the system jumps from a chaotic state to another chaotic state, which is shown in the green domain of Fig. 13(c). In this time, $LE_1 = 0.051$, $LE_2 = 0.0062$, $LE_3 = -0.035$, $LE_1 + LE_2 + LE_3 > 0$, the system is an unstable chaotic state. When $t \in (200,600)$, the system displays a clear three periods, which is shown in the red domain of Fig. 13(c). The corresponding phase diagram is shown in Fig. 13(d). With the parameter k increasing, when $k = 0.47$, $t \in (0,220)$, the system is a single period state, which is shown in the blue domain of Fig. 13(e). Then $t \in (220,600)$, the system jumps from chaos I to chaos II state, which is shown in green and red domains of Fig. 13(e). The corresponding phase diagram is shown in Fig. 13(f).

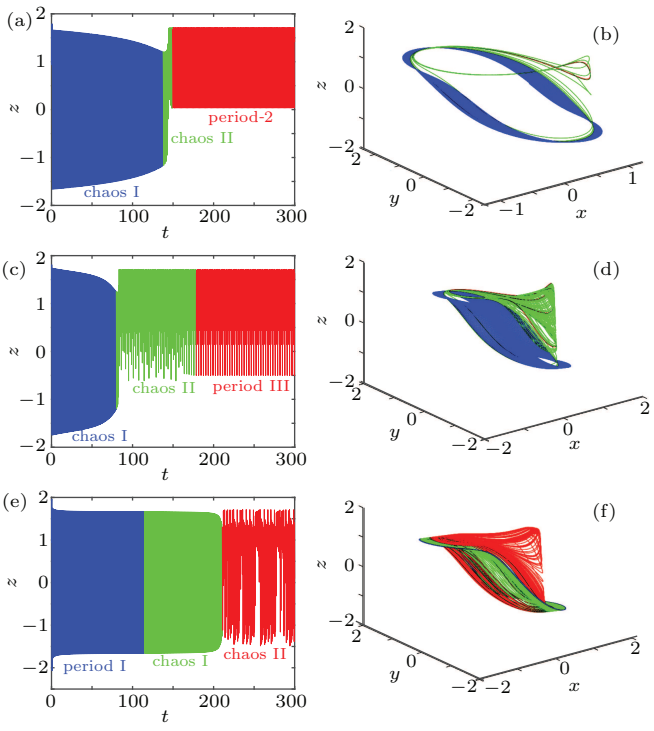

Fig. 13. The time-domain waveform and phase diagram of variable z, (a) $k = 0.06$ time-domain waveform, (b) $k = 0.06$ phase diagram, (c) $k = 0.15$ time-domain waveform, (d) $k = 0.15$ phase diagram, (e) $k = 0.47$ time-domain waveform, (f) $k = 0.47$ phase diagram.

4.4.2. Transient transition when parameter b changes

When the parameter b changes, we firstly fix the parameters $\alpha = 0.8$, $a = 4$, $c = 0.5$, $k = 0.5$ and initial value (1 ,1 ,1), then vary the parameter $b \in (-8, 1.59)$.

Setting $b = -5.4$, the simulation time $t \in (0,600)$, the time-domain wave and phase diagram of the state variable z are shown in Figs. 14(a) and 14(b). When $t \in (0,60)$, the time-domain wave is shown in the blue domain of Fig. 14(a), which indicates that the system is in cycle state, and the range of amplitude is $(-1.5, 1.5)$.

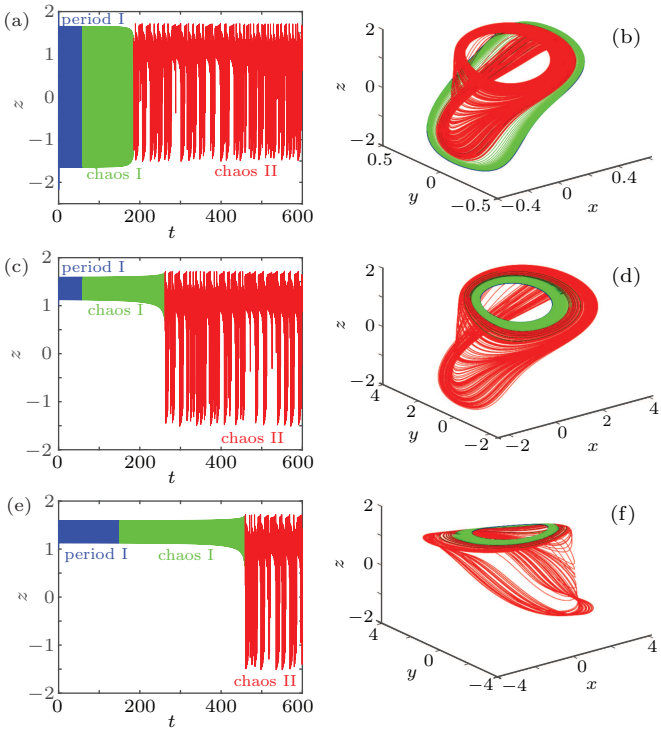

Fig. 14. The time-domain waveform and phase diagram of variable z, (a) $b = -5.4$ time-domain waveform, (b) $b = -5.4$ phase diagram, (c) $b = -0.73$ time-domain waveform, (d) $b = -0.73$ phase diagram, (e) $b = 0.556$ time-domain waveform, (f) $b = 0.556$ phase diagram.

When $t \in (60,180)$, the time-domain wave is shown in the green domain of Fig. 14(a), the system is in chaotic state. When $t \in (180,600)$, the time-domain wave is shown in the red domain of Fig. 14(a). The corresponding phase diagram is shown in Fig. 14(b). When $b = -0.73$, the time-domain wave in $t \in (0,50)$ is shown in the blue domain of Fig. 14(c), and the system is in cycle state, the rang of amplitude is (1.1, 1.5). Then $t \in (50,250)$, the time-domain wave is shown in the green domain of Fig. 14(c), the system is chaotic state. When $t \in (250,600)$, the time-domain wave is shown in the red domain of Fig. 14(c), which shows the system jumps from one chaotic state to another chaotic state. The corresponding phase diagram is shown in Fig. 14(d). With the parameter b increasing, when $b = 0.556$, $t \in (0,150)$, the time-domain wave is in a single period state, which is shown in the blue domain of Fig. 14(e), then $t \in (150,450)$, the system jumps from one period to chaos I state, which is shown in the green domain of Fig. 14(e). When $t \in (450,600)$, the system changes from one chaotic state to another chaotic state, which is shown in the red domain of Fig. 14(e). The corresponding phase diagram is shown in Fig. 14(f).

4.4.3. Transient transition when parameter α changes

To study the rich transient behavior when the parameter α changes, we firstly fix the parameters $a = 4$, $c = 0.5$, $k = 0.5$, $b = 1.5$ and initial value (1 ,1 ,1), then choose the parameters $\alpha \in (0.5, 1)$.

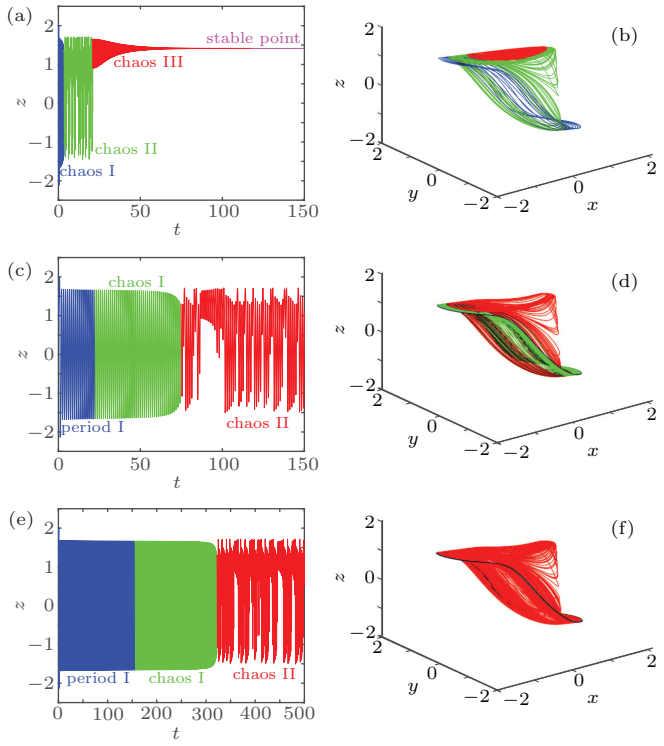

Fig. 15. The time-domain waveform and phase diagram of variable z, (a) $\alpha = 0.6$ time-domain waveform, (b) $\alpha = 0.6$ phase diagram, (c) $\alpha = 0.77$ time-domain waveform, (d) $\alpha = 0.77$ phase diagram, (e) $\alpha = 0.79$ time-domain waveform, (f) $\alpha = 0.79$ phase diagram.

Setting $\alpha = 0.6$, the simulation time $t \in (0, 150)$, the time-domain wave and phase diagram of the state variable z are shown in Figs. 15(a) and 15(b). When $t \in (0, 5)$, the time-domain wave is shown in the blue domain of Fig. 15(a), which indicates that the system is in a chaotic state. When $t \in (5, 25)$, the time-domain wave is shown in the green domain of Fig. 15(a), and the system is in second type of chaotic state. When $t \in (25, 110)$, the time-domain wave is shown in the red domain of Fig. 15(a), the system is in third type of chaotic state. When $t \in (110, 150)$, the time-domain wave is shown in the pink domain of Fig. 15(a), and the system converges to a point. The corresponding phase diagram is shown in Fig. 15(b). When $\alpha = 0.77$, at $t \in (0, 20)$, the time-domain wave is shown in the blue domain of Fig. 15(c), and the system is in a single period state. When $t \in (20, 70)$, the time-domain wave is shown in the green domain of Fig. 15(c), and the system is in a chaotic state. Then $t \in (70, 150)$, the time-domain wave is shown in the red domain of Fig. 15(c), and the system is in another chaotic state. The corresponding phase diagram is shown in Fig. 15(d). With the parameter α increasing, when $\alpha = 0.79$, $t \in (0, 150)$, the time-domain wave is shown in the blue domain of Fig. 15(e), and the system is in a single period state. When $t \in (150, 320)$, the time-domain wave is shown in the green domain of Fig. 15(e), and the system is in a chaotic state. Then $t \in (320, 500)$, the time-domain wave is shown in the red domain of Fig. 15(e), and the system is in another chaotic state. The corresponding phase diagram is shown in Fig. 15(f).

It can be seen that system (17) transits from a state to another state, and finally stabilizes under the above parameters. There are two, three or four states from the beginning to the stable state, which is different from the transient transition behaviors reported in the literature.

5. Implementation on ARM

We implement the fractional-order bi-stable memristive simplest chaotic system on ARM platform. For hardware design, the block diagram of the working principle is shown in Fig. 16. In the experiments, the ARM-based MCU STM32F750 is employed. STM32F750 is a 32-bit ARM-based MCU running at 216 MHz with floating-point calculation unit. The processor comes with a 12-bit/8-bit dual channels digital-to-analog converter (DAC). Phase portraits of the system are captured randomly by an analog oscilloscope. The platform to implement the chaotic system (17) is shown in Fig. 17.

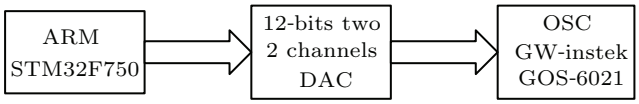

Fig. 16. Block diagram for ARM implementation of a fractional-order chaotic system.

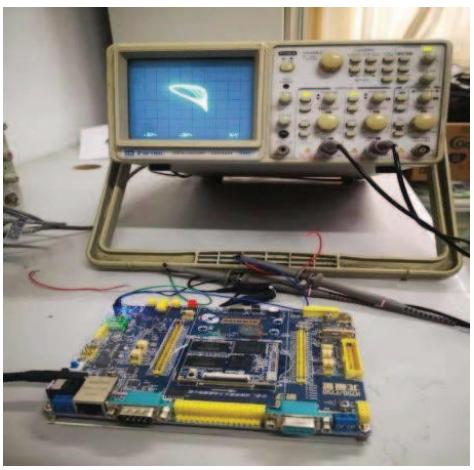

Fig. 17. Platform to implement a fractional-order chaotic system.

The operational procedure of software design is shown in Fig. 18. After initializing ARM, we set the initial values (x_0, y_0, z_0), parameters h, α and iteration number. Before iterative computation, we calculate all $\Gamma(\cdot)$ and $h^{n\alpha}$. Finally, all the data is transferred to DAC and shown in oscilloscope.

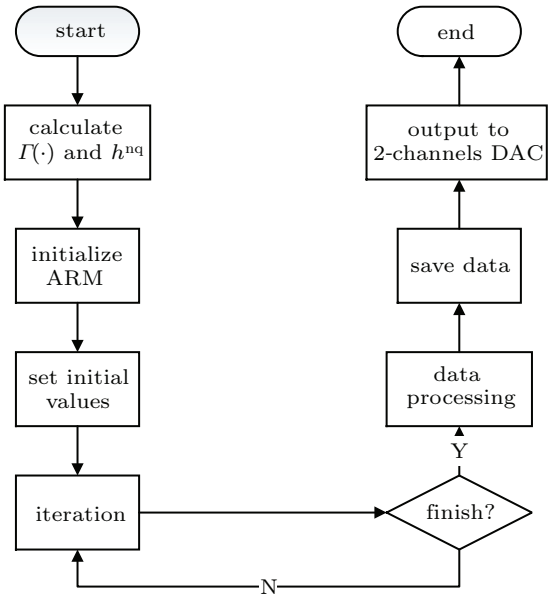

Fig. 18. Flow chart for ARM implementation of a fractional-order chaotic system.

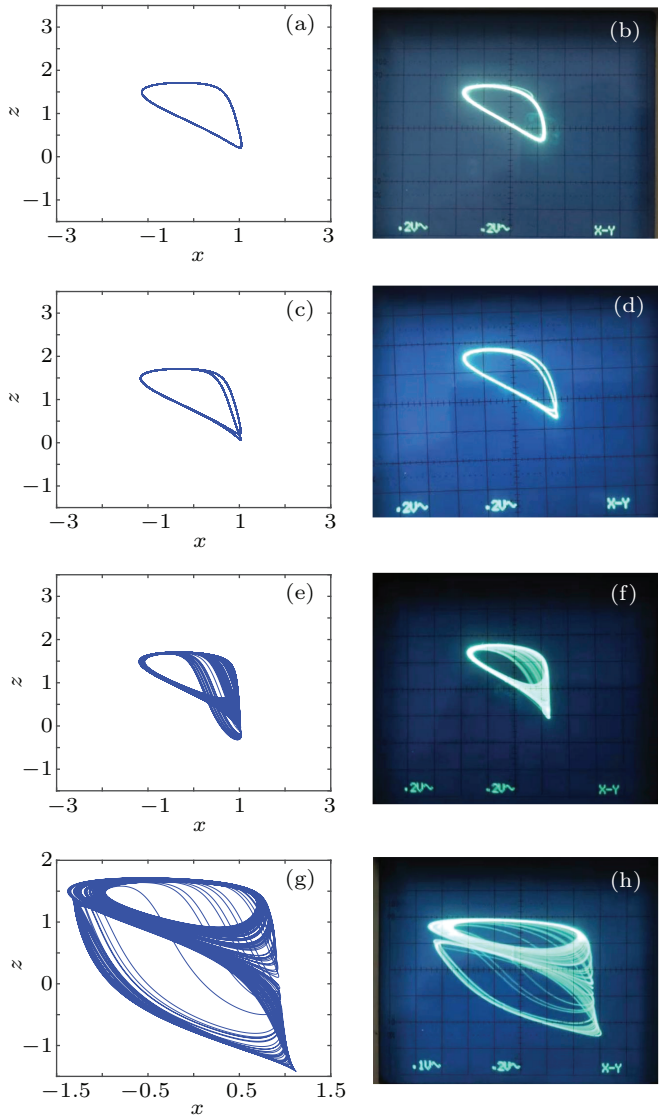

Fig. 19. Phase diagrams realized by ARM platform and recorded by the oscilloscope in x–z plane: (a) $k = 0.1$, (b) $k = 0.15$, (c) $k = 0.2$, (d) $k = 0.45$.

We set $a = 4$, $c = 0.5$, $b = 1.5$, $\alpha = 0.8$, $h = 0.01$, initial values $(x_0, y_0, z_0) = (1, 1, 1)$, and change the parameter k. Phase portraits of the system are captured by the oscilloscope as shown in Fig. 19. The experimental results qualify the simulation analysis. It indicates that the fractional-order bi-stable memristive simplest chaotic system is realized successfully on ARM platform.

6. Conclusion

In this paper, a bi-stable locally-active memristor is firstly proposed, which has double coexisting pinched hysteresis loops and locally-active regions. Then, a fractional-order chaotic system based on the bi-stable locally-active memristor is explored, and the stability of equilibrium points of the system is analyzed. It is found that oscillations occur only within the locally-active region. By bifurcation analysis and Lyapunov exponent spectrum analysis, we find that the system has extremely rich dynamics, such as transient transition behaviors. Finally, the circuit simulation of the fractional-order bi-stable locally-active memristive chaotic system is implemented on ARM-based MCU to verify the validity of the numerical simulation results.

References

[1] Chua L O 1971 *IEEE Trans. Circuit Theory* **18** 507
[2] Strukov D B, Snider G S, Stewart D R and Williams R S 2008 *Nature* **453** 80
[3] Yao W, Wang C H, Cao J D, Sun Y C and Zhou C 2019 *Neurocomputing* **363** 281
[4] Rajagopal K, Parastesh F, Azarnoush H, Hatef B, Jafari S and Berec V 2019 *Chaos* **29** 043109
[5] Lin H R, Wang C H, Sun Y C and Yao W 2020 *Nonlinear Dyn.* **100** 3367
[6] Han X, Sun B W, Xu R X, Xu J, Hong W and Qian K 2021 *Chinese J. Inorg. Chem.* **37** 577
[7] Strukov D B 2016 *Appl. Phys. A* **122** 302
[8] Pabst O, Martinsen R G and Chua L O 2019 *Sci. Rep.* **9** 19260
[9] Zhou L, Wang C H and Zhou L L 2017 *Int. J. Circ. Theor. Appl.* **46** 84
[10] Li C B, Thio W J C, Lu H H C and Lu T A 2018 *IEEE Access* **6** 12945
[11] Muthuswamy B and Chua L O 2010 *Int. J. Bifurcat. Chaos* **20** 1567
[12] Zhan K,Wei D, Shi J H and Yu J 2017 *J. Electronic Imaging* **26** 013021
[13] Yu F, Zhang Z N, Liu L, Shen H, Huang Y Y, Shi C Q, Cai S, Du S C and Xu Q 2020 *Complexity Special Issue* **2020** 5859273
[14] Chai X L, Gan Z H, Yuan K, Chen Y R and Liu X X 2019 *Neural Comput. Applic.* **31** 219
[15] Xu K D, Li D H, Jiang Y N and Chen Q 2021 *Front. Phys.* **9** 648737
[16] Huang Y C, Liu J X, Harkin J, McDaid L and Luo Y L 2021 *Neurocomputing* **423** 336
[17] Liu Y, Guo Z, Chau T K, Lu H C and Si G Q 2021 *Int. J. Circ. Theory Applic.* **49** 513
[18] Yu F, Qian S, Chen X, Huang Y Y, Liu L Shi C Q, Cai S, Song Y and Wang C H 2020 *Int. J. Bifurcat. Chaos* **30** 2050147
[19] Korneev I A, Vadivasova T E and Semenov V V 2017 *Nonlinear Dyn.* **89** 2829
[20] Amador A, Freire E, Ponce E and Ros J 2017 *Int. J. Bifurcat. Chaos* **27** 17300221
[21] Zhu B M, Fan Q H, Li G Q and Wang D Q 2021 *Analog Integr. Circ. Sig. Process* **107** 309
[22] Wang Z L, Min F H and Wang E R 2016 *AIP Advances* **6** 095316
[23] Chen C J, Chen J Q, Bao H, Chen Mo and Bao B C 2019 *Nonlinear Dyn.* **95** 3385
[24] Xie W L, Wang C H and Lin H R 2021 *Nonlinear Dyn.* **104** 4523

[25] Zhu M H, Wang C H , Deng Q L and Hong Q H 2020 *Int. J. Bifurcat. Chaos* **30** 2050184

[26] Gu M Y, Wang G Y, Liu J B, Liang Y, Dong Y J and Ying J J 2021 *Int. J. Bifurcat. Chaos* **31** 2130018

[27] Ascoli A, Demirkol A S, Tetzlaff R, Slesazeck S, Mikolajick T and Chua L O 2021 *Front. Neurosci.* **15** 651452

[28] LiZ J, Zhou H Y, Wang M J and Ma M L 2021 *Nonlinear Dyn.* **104** 063154

[29] Zhu M H, Wang C H, Deng Q L and Hong Q H 2020 *Int. J. Bifurcat. Chaos* **30** 2050184

[30] Klaus M and Chua L O 2013 *Local Activity Principle* (Imperial College Press) pp. 146–159

[31] Itoh M and Chua L O 2008 *Int. J. Bifurcat. Chaos* **18** 3183

[32] Chua L O 2005 *Int. J. Bifurcat. Chaos* **15** 3435

[33] Chua L O, Sirakoulis G C and Adamatzky A 2019 *Handbook of Memristor Networks* (Switzerland Cham: Springer Nature Switzerland AG) p. 89

[34] Mannan Z I, Choi H and Kim H 2016 *Int. J. Bifurcat. Chaos* **26** 1630009

[35] Dong Y J, Wang G Y, Chen G R, Shen Y R and Ying J J 2020 *Commun. Nonlinear Sci. Numer. Simul.* **84** 105203

[36] Jin P P, Wang G Y, Lu H H and Fernando T 2018 *IEEE Transactions on Circuits and Systems II: Express Briefs* **65** 17524546

[37] Ying J J, Liang Y, Wang J L, Dong Y J, Wang G Y and Gu M Y 2021 *Chaos, Solitons & Fractals* **148** 111038

[38] Ying J J, Liang Y, Wang G Y,Iu H H C,Zhang J and Jin P P 2021 *Chaos* **31** 063114

[39] Ivo P, Chen Y Q and Calvin C *2009 IEEE Conference on Emerging Technologies & Factory Automation*,September 22–25, 2009, Palma de Mallorca, Spain, p. 1

[40] Yu Y J and Wang Z H 2015 *Acta Phys. Sin.* **64** 238401 (in Chinese)

[41] Fouda M E and Radwan A 2015 *Circuits Syst. Signal Process.* **34** 961

[42] Yu Y J and Chen Y Q *15th IEEE/ASME International Conference on Mechatronic and Embedded Systems and Applications* August 18–21, 2019, Anaheim, California, USA, p. 7

[43] Wang S F and Ye A Q 2020 *Symmetry Special Issue* **12** 437

[44] Tan Y M and Wang C H 2020 *Chaos* **30** 053118

[45] Yu Y J, Bao H, Shi M, Bao B C, Chen Y Q and Chen M 2019 *Complexity Special Issue* **2019** 2051053

[46] Ying J J, Wang G Y, Dong Y J and Yu S M 2019 *Int. J. Bifurcat. Chaos* **29** 1930030

[47] Gibson G A, Musunuru S, Zhang J M, Vandenberghe K, Lee J, Hsieh C C, Jackson W, Jeon Y,Henze D, Li Z Y and Williams R S 2016 *Appl. Phys. Lett.* **108** 023505

[48] Gorenflo R and Mainardi F 1997 *Fractional calculus: integral and differential equations of fractional-order* (New York: Springer Verlag) pp. 223-276

[49] Podlubny I 1999 *Fractional Differential Equations* (San Diego: Academic Press) p. 88

[50] Chua L O 1993 *Communications and Computer Sci.* **E76-A** 704

[51] Muthuswamy B and Chua L O 2010 *Int. J. Bifurcat. Chaos* **20** 1567

[52] Ahmed E, El-Sayed A M A and El-Saka H A A 2007 *J. Math. Anal. Appl.* **325** 542

[53] Adomian G 1990 *Math. Comput. Model* **13** 17

[54] Bremen H F V, Udwadia F E and Proskurowski W 1997 *Physica D* **101** 1

[55] Chithra A, Fonzin Fozin T, Srinivasan K, Mache Kengne E R, Tchagna Kouanou A and Raja Mohamed I 2021 *Int. J. Bifurcat. Chaos* **31** 2150049

[56] Du C H, Liu L C, Zhang Z P and Yu S X 2021 *Nonlinear Dyn.* **104** 765